Irish Geography
Vol. 52, No. 1 May 2019
DOI: 10.2014/igj.v51i2.1378

Geographical Society of Ireland
An Cumann Tíreolaíochta na hÉireann

Bull Island: characterisation and development of a modern barrier island triggered by human activity in Dublin Bay, Ireland

Sojan Mathew[1*], Xavier M. Pellicer [2], Silvia Caloca[2], Xavier Monteys[3], Mario Zarroca[4], Diego Jiménez-Martín[5]

[1] School of Geography, University College Dublin, Belfield, Dublin, Ireland.

[2] Geological Mapping Unit, Geological Survey of Ireland, Haddington Road, Dublin, Ireland.

[2] Geological Mapping Unit, Geological Survey of Ireland, Haddington Road, Dublin, Ireland.

[3] Coastal and Marine Unit, Geological Survey of Ireland, Haddington Road, Dublin, Ireland.

[4] Àrea de Geodinàmica Externa i Hidrogeologia, Universitat Autònoma de Barcelona, Barcelona, Spain.

[5] TSUP Pesca y Asuntos Marítimos, Pesca Y Asuntos Marítimos / G.Pesca Y Asuntos Maritimos, Grupo Tragsa – SEPI, Spain.

First received: 21 July 2018 *Accepted for publication: 03 April 2019*

Abstract: Bull Island is a 5km long sand spit extending north-eastwards from the North Wall of Dublin Port, and was developed following the construction of the North Wall during the first half of the 19th century. In this investigation, characterisation of hydrostratigraphic units and erosion/accretion rates of the beach dune system was quantified using geomorphological and geophysical data. Depth-to-bedrock and spatial distribution of the major hydrostratigraphic units were estimated from ERT data. GPR data was used to characterise the aeolian sediment thickness and facies associations. It was found that the sediment accumulation in the south-western parts is expressed by low frequency, poorly developed dune ridges of 1-2m height combined with fresh water marshes, evolving north-eastwards into high frequency well-developed sand dunes reaching maximum heights of 9m. DSAS programme aided in estimating the erosion/accretion rates of ca. 3.7m.a^{-1} in the south-western region, ca. 1.2m.a^{-1} along the central portion and ca. 3.4m.a^{-1} along the north-eastern shoreline. The major controls on the evolution of the beach dune system may be ascribable to the sediment supply and hydrodynamic processes in Dublin bay paired with the position of the Dublin Port North Wall.

Keywords: *shoreline, foredune, erosion/accretion, aerial photography, GPR, ERT, geomorphology*

*sojan.mathew@ucd.ie (corresponding author)

Introduction

Sandy coastal systems are particularly dynamic depositional environments, as morphological processes act on a range of temporal and spatial scales, and interactions between processes are very complex. These systems are subject to on-going processes that control erosion, transport and deposition at timescales from minutes to decades and longer (Davidson-Arnott, 2005; Mathew *et al.,* 2010; Houser and Mathew, 2011; Ahn *et al.,* 2017; Johnstone *et al.,* 2016). In addition, they offer excellent opportunities for studies of short-term, small-scale, process-form relationships as well as long-term, large-scale, coastal evolution. Important features of most sandy beach systems are coastal dunes, which are especially responsive to changes in the nearshore/beach dune system and are a significant source of sediment that can regulate the system evolution. Foredunes act as a buffer against wind and waves during storms, protect the land behind them from saltwater intrusion, and function as a reservoir of sand that replenishes or maintains the nearshore/beach dune system during periods of erosion (Aagaard *et al.,* 2004; Paine *et al.,* 2012; Kandrot *et al.,* 2016; Blue *et al.,* 2017). Therefore, understanding these natural landforms and the processes controlling them are very important to the management of sandy coastal ecosystems.

The availability of historic aerial photographic data for the last 80 years, enables us to quantify coastal erosion and geomorphic evolution on a decadal scale. Aerial photographs record the location of the beach at the time the photographs are made and, in addition, show natural and man-made features adjacent to the beach dune system. Analysis of coastal geomorphic change and shoreline erosion/accretion trends using historic/recent aerial photographs are fundamental to a broad range of investigations (Forbes *et al.,* 2004; Mathew *et al.,* 2010; Houser and Mathew, 2011; Paine *et al.,* 2012; Ollerhead *et al.,* 2012; Eulie *et al.,* 2017) undertaken by coastal scientists, coastal engineers, and coastal managers. These data are important in developing sediment budgets, monitoring engineering modifications to a beach (Forbes *et al.,* 2004; Paine *et al.,* 2012), examining geomorphic variations in the coastal zone, studying the role of natural processes in altering shoreline position, establishing setback lines (Paine *et al.,* 2012; Ahn *et al.,* 2017; Johnstone *et al.,* 2016) and predicting future shoreline change through mathematical modelling (Brunn, 1962; Davidson-Arnott, 2005; Mathew *et al.,* 2010; Blue *et al.,* 2017). Aerial photographs beginning in the 1950s are available for most Irish shorelines from the archives of Ordnance Survey of Ireland (OSI) and are used in the current investigation for quantitative measurements of shoreline change rates and landform changes observed, as well as for identifying major geomorphic control on the evolution of the Bull Island sand spit.

The integration of electrical and electromagnetic geophysical techniques as complementary tools for unconsolidated sediments characterisation has been widely explored during the last decade (e.g., Jol *et al.,* 1994; Defranco *et al.,* 2009; Coulouma *et al.,* 2013, Zarroca *et al.,* 2014). In Ireland, GPR surveys have proven successful in the investigation of soft sediments by detecting subsurface discontinuities ascribable to changes of the texture, lithology, internal architecture or the water table (Tronicke *et al.,*

1999; Pellicer and Gibson, 2011; Zarroca *et al.,* 2014). However, the application of GPR surveys in the investigation of coastal aeolian sediments (e.g., Jol *et al.,* 1994; Bristow *et al.,* 2000; Neal *et al.,* 2002; Havholm *et al.,* 2004; Buynevich *et al.,* 2007; Bennet *et al.,* 2009; Cunningham *et al.,* 2011; Choi *et al.,* 2014) are not widely attempted along Irish coastlines. Furthermore, ERT surveys applied to the investigation of the fresh/saline water interface in coastal regions (e.g., Cassiani *et al.,* 2006; de Franco *et al.,* 2009; Zarroca *et al.,* 2011) and depth-to-bedrock detection (e.g., Schrott and Sass, 2008; Coulouma *et al.,* 2013) are not that common in Ireland.

This paper presents a case study of the temporal and spatial patterns of shoreline evolution and coastal geomorphic changes along a 5km stretch of Bull Island, County Dublin, Ireland using historic/recent aerial photographs and digital elevation models (DEMs). In addition, geotechnical data combined with the geophysical methods such as GPR and ERT were used to characterise the subsurface architecture of the sand spit and to identify major hydrostratigraphic units and depth to bedrock within the beach dune system.

Study Area

Bull Island is a sand spit located in Dublin Bay on the north-east coast of Ireland (Figure 1). It is a wedge-shaped, narrow portion of sandy beach system orientated south-west-north-east about 5km long and parallel to the mainland coastline. The system ranges in width between 1km at its south-west and 200m to the north-east end. It encompasses a continuous modern foredune system ranging in height from 2-4m along the proximal end to more than 9m above ordnance datum (OD) in the central-northeast region towards the distal end.

Prevailing wind direction across the study area is from the south and west, while winds from the north-east or north occur least often. In January, the southerly and south-easterly winds are more prominent than in July, which has a high frequency of westerly winds. Easterly winds occur most often between February and May and are commonly accompanied by dry weather (MET Éireann, 2017)

Bull Island is connected to the mainland in two locations, at the south-west end by a wooden bridge linking the Dublin Port North Wall to the mainland and by a Causeway road, constructed during the 1960s, at its central part. The island is banked against the Dublin Port North Wall to the south-west and bounded by Sutton Creek to the north-east, a deep narrow marine channel exists between the distal end of Bull Island and the south coast of Howth Peninsula. The development of Bull Island during the last two centuries was triggered by the construction of the Dublin Port South Wall at the start of the 19th century, prompting the development of a narrow ribbon of supra tidal sand bar prograding south-eastwards into the harbour. This forced the construction of the Dublin Port North Wall at the end of the 19th century (Harris, 1977) to protect infill of the navigation channel of the River Liffey. Bull Island can be divided in three main physiographic units distributed parallel to the coast from nearshore to the lagoon on lee

side: (i) a wide sandy beach with a nearly flat profile at the south-east margin of the island; (ii) a large sand dune area, wider to the south-west gradually narrowing north-eastwards partially disturbed by the development of two golf links at the south and mid regions of the island; and (iii) a flat salt marsh area along the north-east margin of the sand spit with an average width of 200m (see Figure 2).

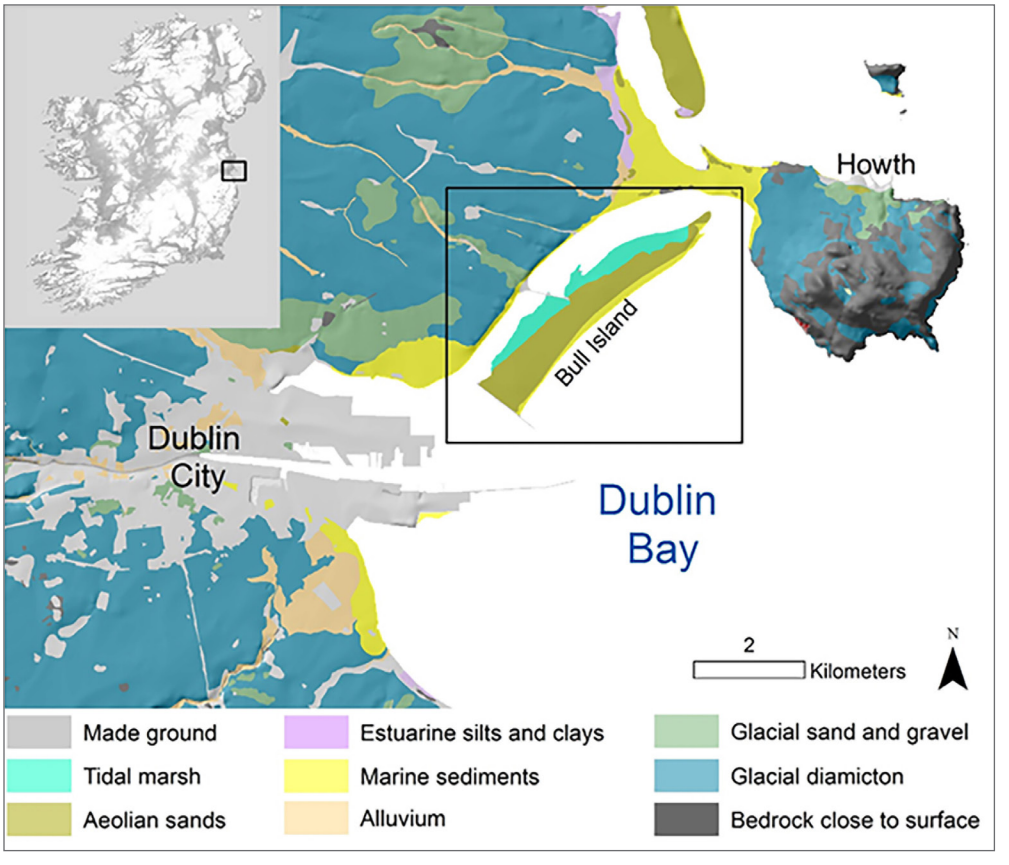

Figure 1: Location of Bull Island and generalised Quaternary sediments distribution in the Dublin Bay area.

Geological and historical context

Dublin Bay is a 10km wide bay enclosed on the north by the Hill of Howth, and on the south by Dalkey Hill. Quartzite rich bedrock of Cambrian age recorded in Howth Peninsula and Granite bedrock outcropping on the Dalkey headland conform the north and south margin of Dublin Bay, respectively. Lower Carboniferous limestone and shale underlie the shallower ground areas within the bay (Harris, 1977; Carter and Orford, 1988). The bedrock in the Dublin Bay region is largely overlain by glacial and post-glacial soft sediments.

The current profile of the County Dublin coastline was mainly shaped during the last glaciation marine isotope (MIS) 2 between ca. 26 ka and ca. 17.3 ka BP (Ballantyne *et al.,* 2006). Three ice sheets/domes interacted in the area during the last glaciation releasing large quantities of glacial and glaciofluvial sediments during ice retreat. This is illustrated by mean minimum average Quaternary sediments thickness in County Dublin of over 4.5m reaching maximums of over 30m in the areas of Dublin Port and Killiney beach (Ballantyne *et al.,* 2006; Pellicer, 2008). The most common deposits in the nearshore of County Dublin are glacial and glaciofluvial sediments derived from Lower Carboniferous Limestone. The Dublin City area where Bull Island developed is mostly underlain by till derived from Lower Carboniferous Limestone, classified on two main members: brown and black boulder clay, where the brown boulder clay has been interpreted as a weathered layer of the black boulder clay (Farrel *et al.,* 1995). Other soft sediments recorded are glaciofluvial sands and gravels, marine sediments and aeolian sediments in the coastal areas as well as fill deposits used to construct the Dublin Port.

The coastal systems in this region can be divided into two main morphological types: (i) flat coast (or graded shoreline) constituted of sandy and gravelly beaches, sand and gravel spits and barriers with associated lagoons, dunes, salt marshes and wetlands as well as the tombolo joining the Howth Peninsula with the mainland; and (ii) cliffed or abrasion coastlines composed of either hard rock cliffs (e.g., Howth Peninsula) and soft sediments cliffs (e.g., Killiney beach) (Carter and Orford, 1988). Hard rock cliffs are morphologically expressed as headlands, whereas soft sediment cliffs undergo intensive erosion processes, evident as a bay-like coastal profile.

The main geomorphological coastal features in County Dublin are presented from north to south: (i) a series of barrier-beach complexes developing at the mouth of estuaries lying between resistant headlands are described along the north County Dublin coastline. These barriers formed as sea levels rose during the postglacial Holocene marine transgression. Unconsolidated glacial clays, sands and gravels were incorporated into coarse grained storm beach ridges, partly closing the bays and creating estuaries behind them (Mulrennan, 1992); (ii) the Howth Peninsula headland is connected to the mainland by a tombolo composed of sand, which formed during a sea-level rise episode about five thousand years ago (Harris, 1977); and (iii) Dublin Bay, flanked by the Howth and Dalkey headlands is dominated by large sand banks at both margins of Dublin Port and culminates in Bull Island by a large sand dune complex.

Methods

In this investigation, a combination of photogrammetric and geophysical methods was used to characterise the evolution of Bull Island. Linear changes in shoreline position and geomorphic units were extracted using photogrammetric methods, and subsequent geospatial analysis was carried out using the geographic information system (GIS) software ArcGIS (version 10.3). In addition, geophysical methods such as GPR was used to characterise beach dune subsurface sediment architecture and ERT in combination

with geotechnical data was used to examine major hydro-stratigraphic units as well as depth to bedrock along the study area.

Data sources

Six sets of historic and recent aerial/satellite imagery taken in 1952, 1971, 1995, 2000, 2005, and 2013 were used to quantify decal scale evolution of the Bull Island. Firstly, black and white contact prints of vertical aerial photographs taken by The Irish Air Corps in 1952 and by OSI in 1972 were digitally scanned at an optical resolution of 600 dpi using a large format Epson GT-30000 flatbed scanner. Scanned images were saved in Geo-Tiff format and pixel resolution ranged from 0.45m to 0.64m (see Table 1). Subsequently, rectification of aerial photographs was attempted using ground control points (GCPs) that link historic images to its corresponding aerial coverage on 1995 orthophoto imagery. As most of the identifiable features on the landscape such as road intersections, trails, monuments and cultural features were missing on historic aerial photographs, finding accurate GCPs, using the earliest available orthophoto imagery (1995), was difficult. To some extent these problems were overcome by carrying out rectification sequentially beginning with 1972 photography. This meant that additional GCPs from rectified 1972 images could be used to supplement the rectification of the 1952 photographs. Once sufficient GCPs were collected, the georeferencing extension tool in ArcGIS 10.3 using 1st order polynomial (affine) transformation was used to generate rectified historic aerial images. RMSE varied from around 3m in the case of 1952 and 2m for 1971 aerial photographs (see Table 1).

In addition, digital orthophotos taken in 1995, 2000, 2005 at 1m resolution and 2013 digital globe imagery at 0.30 m were obtained from OSI. As RMSE report for the above dataset was not available, a real time kinematic (RTK) differential GPS survey was conducted using identifiable features as GCPs. As evident in Table 1, RMSE ranged from 0.6 in the case 2013 digital globe imagery and 1.6 m for 1995 aerial photographs. Moreover, high resolution lidar DEM, collected by the Office of Public Works (OPW) in 2006 with vertical accuracy of ± 0.15m at 2m pixel resolution, were used to delineate major geomorphic features across the study area.

Note that the geospatial data used in this investigation were referenced to the European petroleum survey group (EPSG) coordinate system 2157 and the details are as follows:

Projection: Irish Transverse Mercator (ITM); Datum: IRENET 95; Ellipsoid: geodetic reference system (GRS) 1980.

Table 1: Details of historic and recent aerial/satellite imagery and lidar data of Bull Island

Year	Source	Media Type	Resolution (m)	RMSE (m)
1952	Air Corps (GSI)	Scanned black and white contact prints @ 600 dpi	0.45	3.2
1971	OSI	Scanned black and white contact prints @ 600 dpi	0.64	2.1
1995	OSI	Digital orthophotos (black and white)	1	1.6
2000	OSI	Digital orthophotos (colour)	1	1.3
2005	OSI	Digital orthophotos (colour)	1	1.2
2006	OPW	Lidar point cloud	2	0.15
2013	OSI	Digital Globe orthoimage (colour)	0.30	0.6

Shoreline mapping and change rates analysis

Detailed mapping and change analysis of shoreline position and geomorphic units were carried out for a 5km distance along the study area. Based on a literature review, a number of shoreline definitions (Moore, 2000; Mathew *et al.,* 2010; Paine *et al.,* 2012; Ollerhead *et al.,* 2012; Johnstone *et al.,* 2016; Ahn *et al.,* 2017; Eulie *et al.,* 2017) have been employed for measurement of shoreline change rates. The most commonly used shoreline reference features (SRF) are high tide line, low tide line, wet/dry line, wrack deposit line, a berm, the beach crest, seaward limit of vegetation, and cliff top as well as dune crest. In this investigation, vegetation line was used as an SRF as it is a less variable indicator of long-term shoreline change, and it could provide an average estimate of the position of seaward limit of vegetation. Moreover, the response of the vegetation line to erosion or accretion was in the order of months to years, rather than the high-frequency changes of the wet/dry line. In this study, six historic vegetation line positions were delineated from orthophoto mosaics of 1952, 1972, 1995, 2000, 2005, and 2013 using Arc GIS software. Subsequently, cross-shore profiles were generated from a shore parallel base line using ArcGIS extension digital shoreline analysis system (DSAS) created by Thieler *et al.,* 2017. The output from DSAS analysis produced 262 shore-perpendicular transects at a spacing of 20m along the study area. Shoreline movement was calculated for every 20m in the alongshore direction from the Dublin Port North Wall to north-eastern end of Bull Island for a total of approximately 262 rate determinations. As the baseline does not exactly mimic the meandering of the shoreline, some transects crossed each other and these were edited out to reduce confusion in the location of shoreline change measurement.

DSAS estimates long-term coastal erosion/accretion rates by means of (i) endpoint rate; (ii) simple linear regression; (iii) weighted linear regression; and (iv) least median of squares. DSAS programme gave long-term rates of change and associated statistics over the last eight decades. Rates were calculated as linear regression rates and net average rates. Where regression coefficients of determination are relatively high, rates calculated

using the linear regression method reasonably express the long-term movement of the shoreline. Where coefficients are low and fitting errors are high, regression rates may not reasonably reflect the long-term movements of the shoreline. In these cases, net rates that represent the simple average rate of change, calculated by dividing the movement distance by the elapsed time, were used. Note that the average annual recession/accession rates were simply referred to as erosion or accretion rates, where positive values denote accretion and negative values denote erosion. Finally, based on historic shoreline change rates, attempts were made to predict the approximate shoreline position in 2067 along each of the transects at 20m intervals.

Geomorphological Evolution

Geomorphological mapping was conducted from an analysis of highly accurate and spatially dense lidar DEM, aerial photography interpretation, and field mapping of Bull Island. The Geophysical methods such as ERT and GPR were used to characterise the subsurface geoelectrical signature and internal architecture. Existing geotechnical investigation records in Bull Island and the Dublin Port were also used to refine the interpretation of GPR and ERT results.

ERT data collection and analysis

The geoelectrical survey encompassed the acquisition of five ERT profiles parallel and perpendicular to the shore line, in three selected sites (Figure 2), using a Tigre 32 resistivity meter (Allied Associates) and 25 or 32 electrodes, spaced at 10m and 5m respectively. The hybrid Wenner-Schlumberger array (WS) was used since it provides an enhanced data coverage, while maintaining a good signal-to-noise ratio (Zarroca *et al.,* 2011, 2014). Resistivity data was processed with the AGI EarthImager 2D inversion software, which is based on the least-square smoothness-damping constrained method (Occam's inversion) (Constable *et al.,* 1987; LaBrecque *et al.,* 1996). The measured apparent resistivity dataset was filtered to remove possible erroneous points. The filtering was carried out prior to the inversion process (e.g., negative voltage or with high coefficient of variation during recording cycles). Once the filtered pseudosection is inverted, the RMSE provides statistical information on the model residuals which is the difference between calculated and modelled pseudosections. Moreover, to assess the measurement errors, stacking methodology was done to help reduce the errors (Peter-Borie, 2011). Stacking was used with four cycles and a quality factor of 5%. In addition, contact resistance values were obtained before data collection. During post processing, attempts were made to achieve a better convergence between measured and computed pseudosections. When the RMS error was high, attempts were also made to achieve a lower RMS error by a rougher data filtering.

GPR data collection and analysis

GPR data was collected using a Geophysical Survey Systems, Inc (GSSI) system with 200 MHz antennae in constant offset mode with receiver and transmitter antennae at 1m distance and a time window of 150ns. The system, including an odometer wheel, allowed for automatic collection of readings at constant 5cm intervals, within the minimum distance between readings recommended in for 200 MHz antennae (Bristow *et al.*, 2000; Neal, 2004). Data were processed using the software packages EkkoView and EkkoView deLuxe. Data processing encompassed the following steps: (i) Velocity calibration based on hyperbolae reflection analysis presented an average velocity of 0.11m/ns. This velocity is within the typical range for well sorted sands (Neal, 2004) and similar to those obtained in alike aeolian coastal environments (e.g., Bristow and Pucillo, 2006, Choi and Kim, 2013); (ii) Automatic time zero adjustment; (iii) high pass (dewow) and low pass filter, using a lower and higher cut off of 25 MHz and 500 MHz, respectively; (iv) application of an Automatic Gain Control (AGC) using a window width of 1, and a maximum gain threshold of 500; and (v) topography correction based on topographic data collected during the GPR surveys using a Trimble RTK GPS system. The processed datasets were interpreted based on the radar facies methodology from Neal (2004) coupled with geomorphological data (Figure 4). The interpretation coding format has been adapted and modified for this project (Figure 4) by using radar facies specific to coastal environments (Bristow *et al.,* 2000; Neal *et al.,* 2002) and representing the internal architecture from aeolian, marine and estuarine environments existing in the Bull Island area.

Results

Geomorphology

Aerial imagery interpretation paired with field mapping allowed the production of a detailed geomorphological map for estimating shoreline change rates. Four main geomorphological units were mapped in Bull Island: (i) a beach complex situated along the foreshore of the south-east coastline; (ii) a sand dune complex covering the higher ground areas; (iii) salt marsh along the north-west coastline; and (v) a sand/mud flat area covering the region between the island and the mainland (Figure 2).

The beach complex is exposed seawards during low tide along the south-east coastline for about 600m in the southern region and reaches a maximum width of 900m in the north-east of the island along Sutton Creek. It is composed of a series of ridges and runnels truncated in places by drainage channels running normal to them and gradually increasing in number towards the north-east parts of the island where the beach profile is less steep.

The sand dune complex located in the central part of the island extends for 5km from south-west to north-east, it consists of 840m wide sand dune complex in the south-west region along the Dublin Port North Wall and gradually thinning to the north-east where it tails off in a recurve constrained to the north-east by Sutton Creek (see Figures 2 and

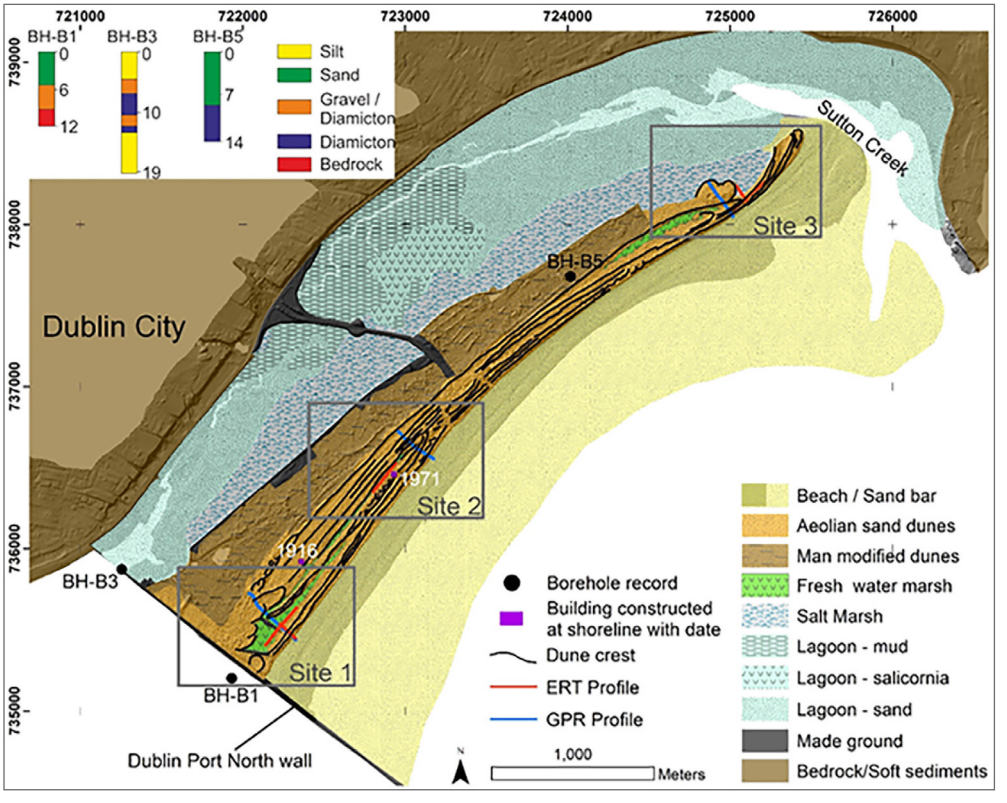

Figure 2: Geomorphology and sediment distribution map for Bull Island. 2m DEM from OPW (which was collected in 2006) is used as topographic background. Borehole logs obtained from the Geological Survey Ireland geotechnical database. Bathing facilities buildings constructed at shoreline in 1916 and 1971 illustrate rapid coastal progradation during the 20th century.

3). Sand dune ridges in the south-west region show poor topographic expression and are often separated by large fresh water marsh areas. These ridges become gradually higher, parallel and better developed north-eastwards as the fresh water marshes gradually wane into the inter-dune areas. Furthermore, a continuous ridge of embryonic dunes developing along the shoreline for over 2.5km indicates on-going accretion processes in the south-east area. Dune ridges lose some continuity in the island middle regions where intense human activity and several blowouts are recognised. North from this region the sand dunes become larger, reaching maximum heights of 9m OD. In this area, two diverging dunes which converge again to the north-east allowed for the development of the Alder Marsh (Figure 3), a fresh water marsh of significant ecological value. In the region to the north-east, where these sand dunes converge in a single dune ridge, an area showing a circular dunes architecture, namely Green Island (Figure 3), is recognised. Green Island precedes the development of the longitudinal sand dune cordons dominating the northern parts of Bull Island. Its formation has been dated to 1869 (Harris, 1977).

This illustrates the existence of a palaeo-coastline over 150 years old. North of Green Island a single foredune ridge diverges out into several ridges forming the recurve at the north-east end of Bull Island.

Salt marsh deposits are recorded along Bull Island north-west coast between the sand dune system and the lagoon flat; a sharp change in slope corresponding to the high-water mark separates it from the lagoon area. The salt marsh is composed of a mixture of sandy mud with plant remains and a series of drainage creeks meandering from the dunes to the lagoon. The lagoon area could be divided into three separate regions: (i) lagoonal mud flat covering the northern margin of the Bull Island causeway; (ii) the salicornia mud flat, which spread largely after the construction of the causeway; and (iii) the lagoonal sand flat areas that are strongly influenced by tidal currents.

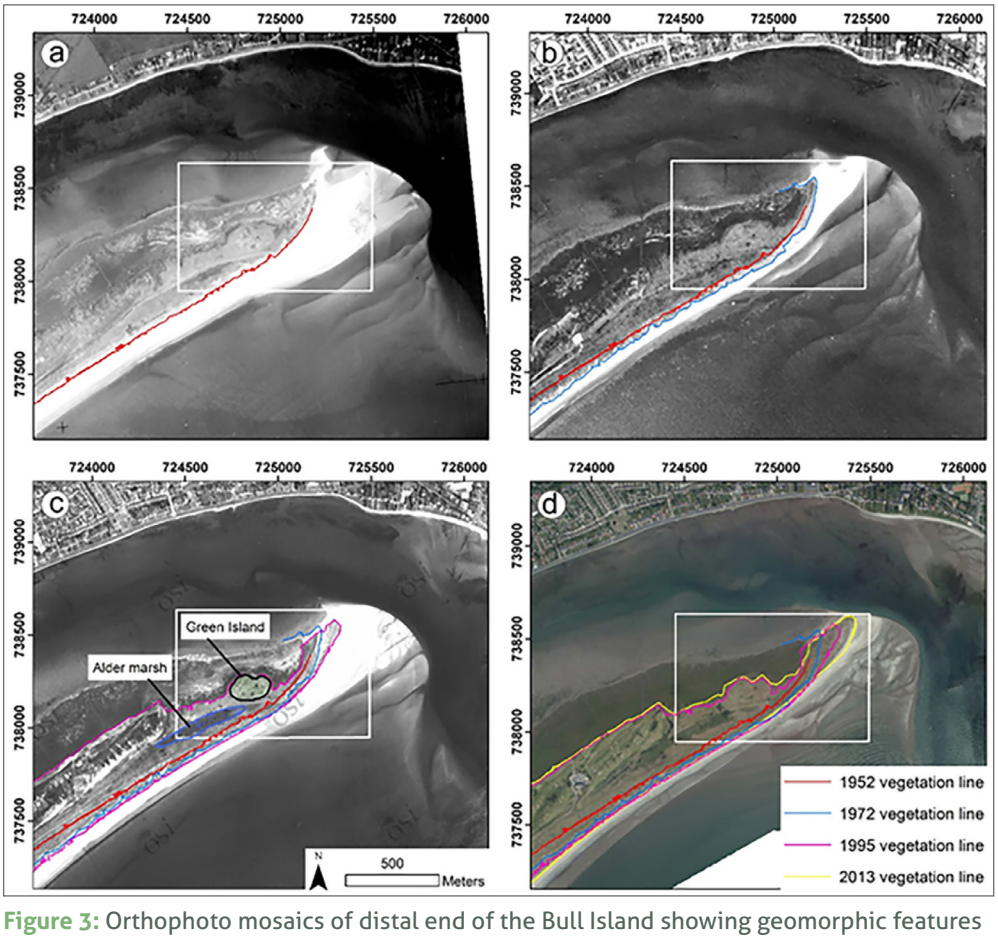

Figure 3: Orthophoto mosaics of distal end of the Bull Island showing geomorphic features in: (a) 1952; (b) 1971; (c) 1995; (d) 2013. Location of Site 3 is shown as a white polygon.

Geophysical surveys

Three sites presenting distinctive geomorphological expressions were selected to carry out geophysical investigations including ERT and GPR surveys (Figure 2). Site 1 was located by the Dublin Port North Wall, Site 2 situated in the middle area, south of the causeway road connecting the island with the mainland, and Site 3 in the north-east region between Green Island and the barrier spit (Figures 2 and 4).

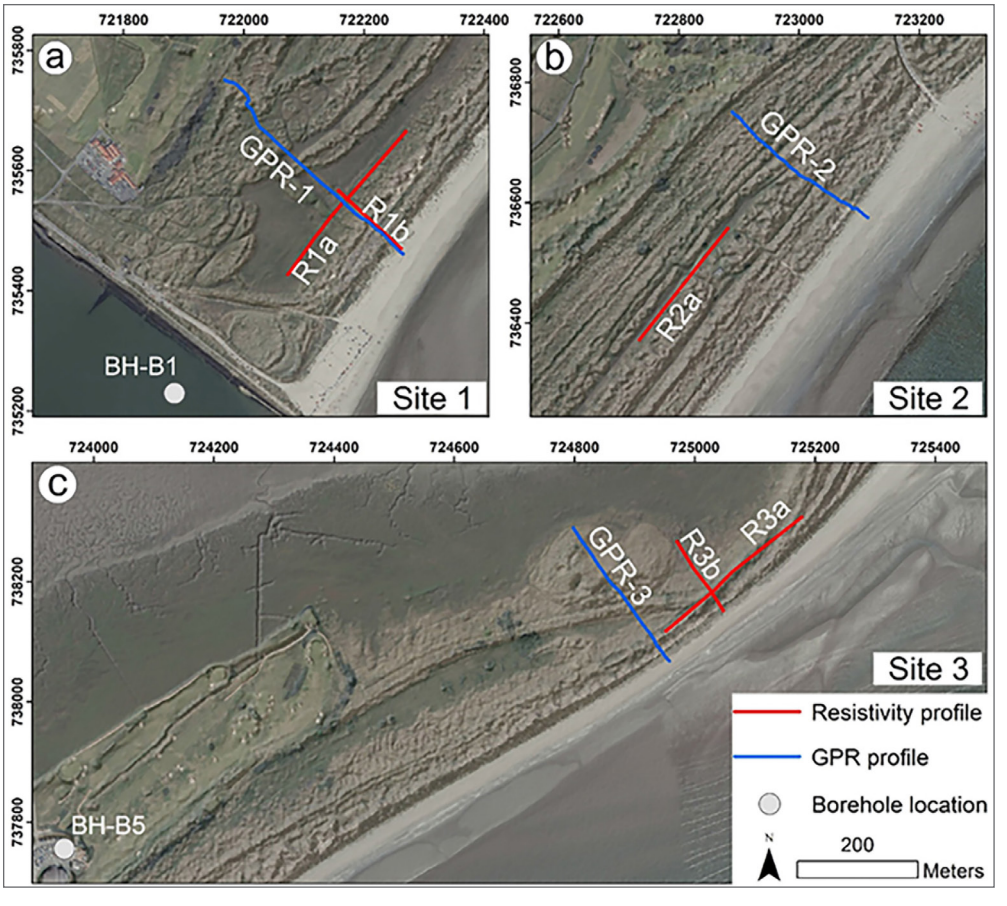

Figure 4: Location of geophysical profiles and boreholes in Site 1, Site 2, Site 3 shown over high resolution 2006 orthophotos.

The joint observation of the processed resistivity images allowed identifying three main electro-units (Figure 5), which may be correlated with the distinct morphostratigraphic units. The uppermost higher-resistivity electro-unit (δ > 100-200 Ωm; reached values over 5000 Ωm) corresponds to the emerged sand dunes package, whose thickness ranges 5-7m. The influence of sediment texture on the bulk resistivity obtained is masked by the pore fluid low-resistivity (Zarroca *et al.*, 2011, 2014). This may cause a relative divergence between the geometry of geoelectric units observed and the actual stratigraphic units.

Therefore, the thickness of the stacking of sand dunes would be underestimated by the resistivity image. The interpretation of the resistivity model has been constrained by geotechnical data BH-B1 and B5 (Figure 4) suggesting that aeolian sediments thickness could reach around 6m in Sites 1 and 2, and up to 9m in Site 3. Underlying the aeolian dunes, the lower resistivity unit ($1 < \delta < 50\ \Omega m$) comprise till deposits of different textures, i.e., clay, gravel and diamiction beds, probably reworked by tidal channels. The higher-resistivity areas identified on the resistivity images might be imaging coarser-gravel units (e.g., profile R2a below x-coordinate 200m; R2a below 210m (see Figures 4, 5), and is consistent with the boreholes BH-B1 and BH-B5. However, these higher resistivities could also be ascribed to inversion artefacts (e.g., Profile R3a, below x-coordinate 105m, Figure 5) or the remains of the shipwrecks reported in the area (Flood, 1975).

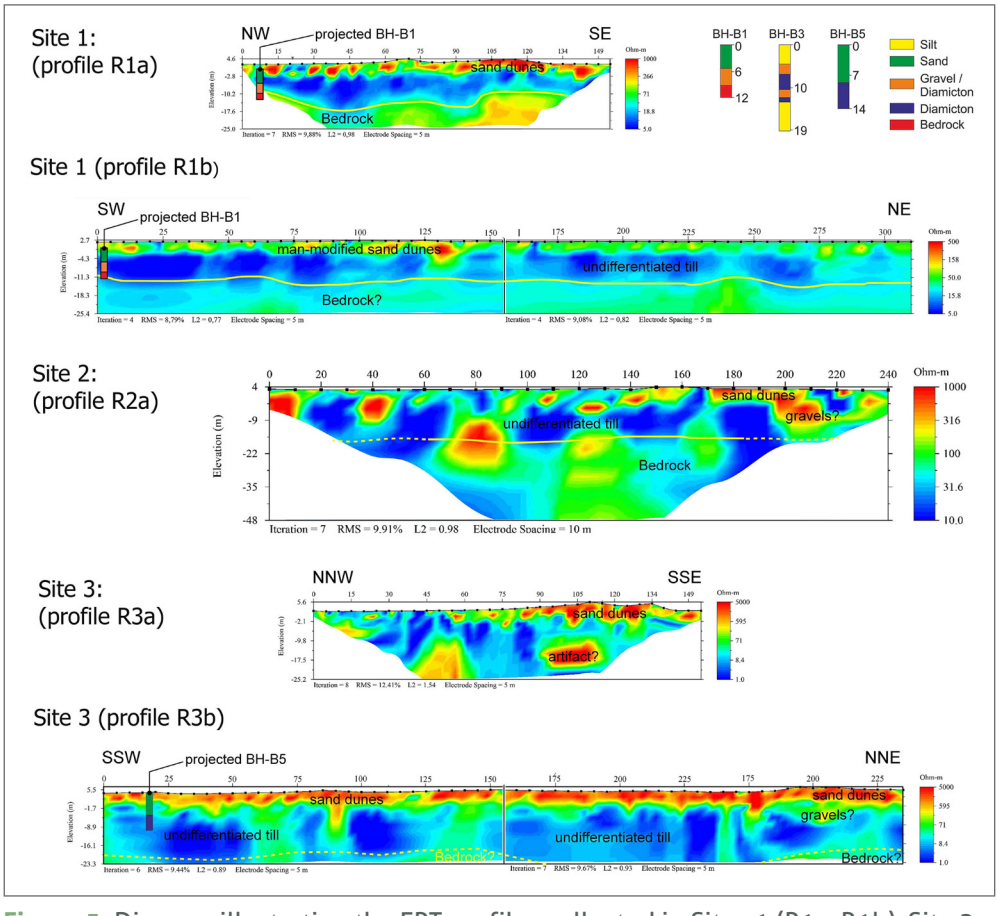

Figure 5: Diagram illustrating the ERT profiles collected in Sites 1 (R1a, R1b), Site 2 (R2a) and Site 3 (R3a, R3b) with their corresponding interpretation. Boreholes log data close to Site 1 and Site 2 (BH-B1) and Site 3 (BH-B5) is shown to the right of resistivity images. Note that the yellow line depicts the inferred interface between the glacial till and bedrock substrate.

Depth-to-bedrock could not be ascertained for the three different sites. The resistivity images of Site 3 (R3a, R3b) depict a gentle increase in the bulk resistivity ($20 < \rho < 100$ Ωm) beneath the elevations -11 to -15m below sea level (bsl) which may delineate the substrate topmost part (Figure 5). This is in concordant with the borehole BH-B1 and BH-B5 logs, and it is much more uncertain for Sites 1 and 2. Alongshore resistivity profile R2a (Site 2) reached a higher investigation depth that enabled modelling up to ca. -50m bsl, although the image does not depict clearly the transition between the lower-resistivity till and the higher-resistivity bedrock. The image suggests that the soft sediments-bedrock interface occurs between -18 to -20m bsl. Nevertheless, some high-resistivity nodes, which may relate to inversion artefacts, mask the probable transition zone. Depiction of depth-to-bedrock is even more difficult in Site 3, since the target is located at the bottom of the modelled depth with poor sensitivity. However, regions with relatively high resistivity below -20m bsl may indicate the presence of bedrock at this depth, which is also consistent with the borehole BH-B5 log (Figure 5).

GPR surveys in Site S1 were taken on a sand dune system showing relatively smooth topographic expression reaching maximums of 2 to 3m height. GPR profile GPR-1 (Figures 4 and 6) running orthogonal to the dunes cut across seven dune ridges separated by large areas underlain by fresh water marsh. The interpreted profile shows six radar facies and embryonic dunes are recorded along the seaward side of the foredunes system. Most of the dunes are composed of foreslope and rearslope accretion deposits with foreslope deposits dominating. The slacks between slopes are either composed of interstratified foreslope and rear-slope deposits and/or bio-topographic accumulation deposits. A large freshwater marsh at 90-180m along the line dominates the interdune region. This marsh was probably dominated by saltwater in the past and was gradually recycled into freshwater as the sand dunes advanced seawards and dams were built to prevent sea water flooding during high tides. A continuous reflector dipping south-east showing continuity under the water table is interpreted as an erosional contact probably illustrating the former coastline. As evident in Figure 5, marine sediments consisting of continuous seaward gently dipping moderately continuous reflectors mostly developed beneath the water-table. These sediments, recorded in borehole BH-B1 (Figure 5), are mostly composed of sand and silty sand.

Sand dunes in Site S2 consist of well-developed subparallel ridges with an average height of 4-5m above the slack area (Figures 4 and 6). GPR Profile GPR-2 running orthogonal to the dunes cut across approximately ten individual ridges separated by slack areas covered in places by narrow minor fresh water marsh sediments. The dunes are generally composed of foreslope and rearslope accretion deposits, the slacks between slopes are either composed of these facies represented by continuous to discontinuous subparallel dipping reflectors and/or bio-topographic accumulation consisting of discontinuous sinuous concave and convex-up reflectors (Figure 6). Reflectors dipping up to 12° towards the south-east, interpreted as foreslope accretion units, are the dominant radar facies. Embryonic dunes are recorded along the seaward side of the foredune system as chaotic discontinuous reflectors. Marine sediments expressed as continuous

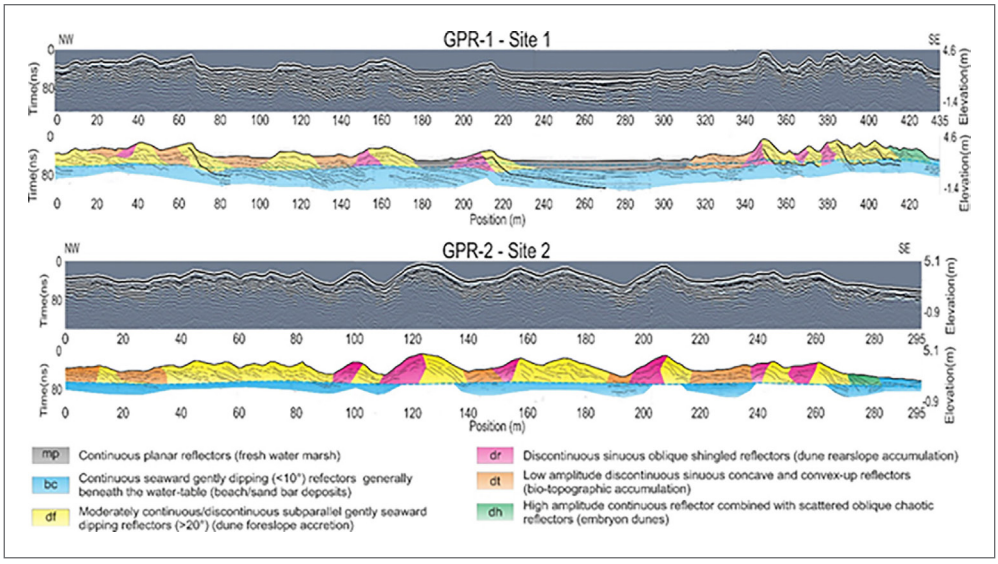

Figure 6a: GPR profiles GPR-1 (Site 1), GPR-2 (Site 2) with corresponding legend. Radar facies interpretation used in the profiles following the methodology from Neal (2004) is presented in Figure 6b.

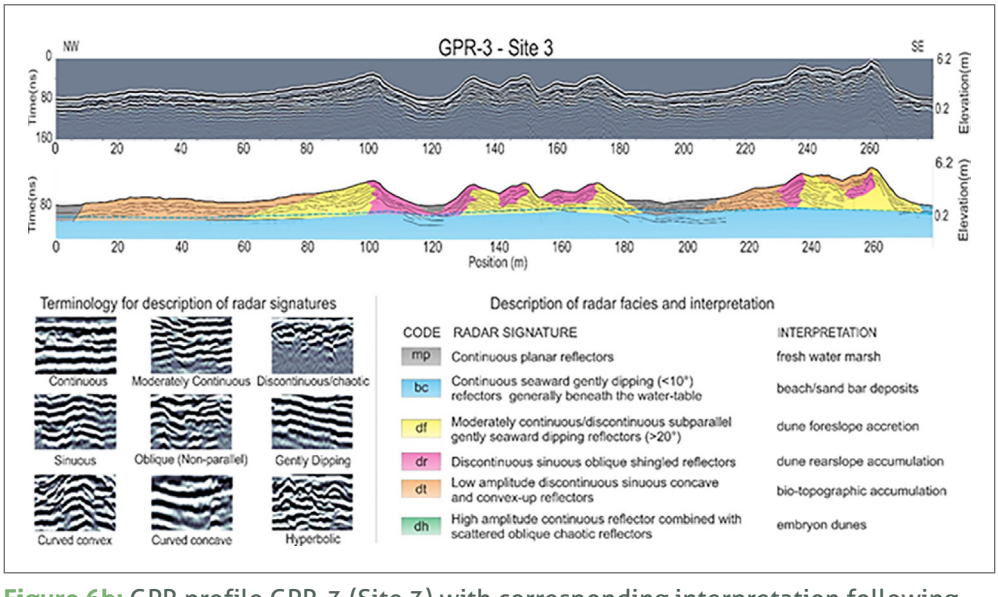

Figure 6b: GPR profile GPR-3 (Site 3) with corresponding interpretation following radar facies interpretation methodology from Neal (2004).

seaward gently dipping moderately continuous reflectors mostly developed beneath the water-table and the underlying sediments are composed of sand and silty sand (Figure 5) as recorded along the intertidal zone (Figure 6).

In Site 3, five radar facies are recognised in GPR profile GPR-3 from reflection character and geometry (Figures 4 and 6). The profile cuts from a salt marsh area to the north-west, Green Island, two parallel continuous sand dunes, a fresh water marsh depression, the current foredune system and beach sands to the south-west. Continuous planar reflectors at 0-5m and 180-210m along the profile are interpreted as salt marsh and fresh water marsh, respectively. Foreslope deposits are represented by moderately continuous/ discontinuous subparallel gently seaward dipping reflectors. Rear slope accumulation consists of discontinuous sinuous oblique shingled reflectors, particularly well developed in the Green Island area. Bio-topographic accumulation facies depicted as low amplitude discontinuous sinuous concave and convex-up reflectors are recorded in the slack of the dunes and as an extensive sand sheet north-west of Green Island. Reflectors dipping gently south-eastwards generally developing below the water table are interpreted as marine beach/sand bar deposits. Sand dunes in the Green Island region show circular foredune development (Figures 4 and 6), confirming this island was probably formed independently at an earlier stage than the parallel dune ridges to the east. The oldest of those truncates the Green Island south palaeo-coastline, the truncation is expressed as a continuous reflector dipping south-east depicted at x-position 155-175m in GPR-3 (Figure 6) and interpreted as an erosional contact illustrating the paleo-coastline in 1905 (Harris, 1980). Most probably, dunes to the south-east of this ridge were formed at a later stage and merged to the east of Green Island as a single ridge.

Shoreline evolution

A detailed investigation of shoreline change-rates was attempted along a 5km stretch of Bull Island along coastal reaches A, B, C, based on the shoreline stability and similarity of geomorphic features (Figure 7a). An overlay of historic shoreline positions and spatial extent of each of the coastal reaches is shown in Figure 7a. Table 2 provides a summary of the statistics of average erosion/accretion rates in each of the coastal reaches between the period 1952-2013.

Mean shoreline change was around 240m along coastal reach A, and the accretion rate was found to be 3.69m.a^{-1}. Eighty-three transects were used for the calculation of the mean accretion rate. A maximum accretion rate of 5.44m.a^{-1} and a minimum accretion rate of 3.13 were found. A standard deviation (SD) of 0.57 shows that the mean accretion rate estimated for 1.6km along this stretch is a reasonable representation.

Shoreline change analysis along reach B depicts a much more stable foredune system. Mean shoreline movement was found to be around 80m and the accretion rate was 1.29m.a^{-1}, which is slower than reach A. One hundred and thirty-two transects were considered in reach B calculations. As is evident in Table 2, a maximum accretion rate of 3m.a^{-1} and a minimum of 0.3m.a^{-1} were found. A standard deviation of 0.73 shows that mean annual accretion rate might be a good representation of 2.6km along reach B.

Table 2: Summary statistics of average annual erosion/accretion rates between the periods 1952 and 2013

Coastal reaches	Mean shoreline change (m)	Mean accretion rate ($m.a^{-1}$)	SD	Max accretion rate ($m.a^{-1}$)	Min accretion rate ($m.a^{-1}$)	Range ($m.a^{-1}$)	No. of transects
Coastal reach A	241.36	3.69	0.57	5.44	3.13	2.31	83
Coastal reach B	81.82	1.19	0.75	2.98	0.28	2.7	132
Coastal reach C (Seaward side)	107.35	3.36	1.45	5.68	1.01	4.67	27
Coastal reach C (Leeward side)	-8.04	-0.38	0.49	0.81	-1.08	1.89	13

In reach C, shoreline accretion rates were calculated separately for the seaward (north-eastern) side and leeward (north-western) side as they were showing a net erosional trend along leeward and accretional trend along seaward side (see Figures 7a and 7b). Along the seaward side and Sutton Creek (Figure 7b), mean shoreline displacement was found to be c.a.100m and accretion rates were estimated as $3.7m.a^{-1}$. There was a greater variability in accretion rates along this section with a maximum of $5.7m.a^{-1}$ and a minimum of $1m.a^{-1}$. This variability is explained further by a larger SD deviation of 1.45. However, shorelines along the leeward (north-western) side shows an erosional trend of 0.4m. A SD of 0.5 confirms further that the estimated erosion rate along the saltmarsh area (north-western) side could be a good estimate of the variability of erosion rates along thirteen transects in reach C.

In this investigation, as explained earlier, historic shoreline change rates along each transect for the period 1952-2013 were used to predict the shoreline position in 2067 (Figure 7b). Close examination of the forecasted shoreline position shows that the north-eastward progradation will slow down and the sand bar along Sutton Creek will recurve more into the eastern side with occasional flooding and sedimentation across salt marsh and lagoon areas. It is anticipated that the shoreline position will be about 50-70m north-eastward (reach C) in 2067. The shoreline in the vicinity of North Bull Wall (reach A) is also predicated to prograde seaward by about 100-150m. As expected, the shoreline position along the central portion of the Island (reach B) will remain stable and regress at a slower rate compare to south-eastern (coastal reach A) and north-eastern (coastal reach C).

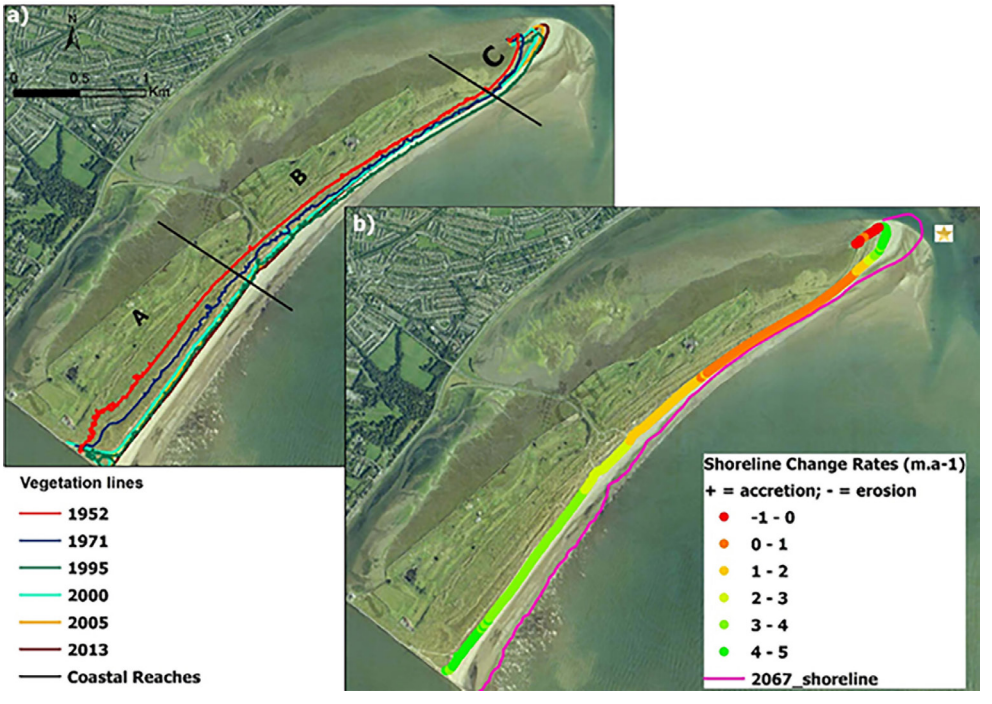

Figure 7: (a) Historic position of shorelines; (b) estimated shoreline change rates along the study area and predicted shoreline position in 2067 based on linear shoreline regression rates. Star denotes the projected shoreline position where the uncertainty is highest.

Discussion

Geomorphological mapping and shoreline change analysis of Bull Island illustrates a sandy spit prograding south-eastwards through the development of a continuous beach dune system fed by a large sand bank exposed to the surface during low tide. These sand dunes are generally more spaced and show lower elevations on the south-western side and gradually become higher and more frequent towards the north-eastern end of the sand spit. There is a growing body of literature (e.g., Mulrennan, 1993; Mathew *et al.,* 2010; Houser and Mathew, 2011; Paine *et al.,* 2012; Johnston *et al.,* 2016; Kandrot *et al.,* 2016; Blue and Kench, 2017) providing insights on the evolution of sandy beach dune systems at different spatio-temporal scales and major controls on their evolution. However, most of these studies were focussed on surface geomorphology using historic aerial photographs and field surveys, and limited attention was paid to subsurface evolution.

A comparison of Bull Island with the map of the North Bull made by Francis Giles in 1819 (Flood, 1975) and orthophotos mosaics of 1952, 1971, 1995, 2000, 2005, and 2013 (Figures 3 and 7), reveals that massive bio-physical changes have taken place in Bull

Island over the past two centuries. Based on aerial photographs in 1952, the vegetation line along coastal reaches was hundreds of metres inland and there were no signs of continuous foredune development above the supra tidal spit platform (Figures 3 and 7). Consistent with the shoreline response models (e.g. Brunn, 1962; Davidson-Arnott, 2005), northward transport of sediment through hydrodynamic processes and fetch limited conditions of the Irish Sea might have permitted the sand ridges to build-up in height along the foreshore and enable stabilisation of ridges through colonisation of native species such as Maram grass. This may have resulted in a continuous foredune system which is more than 9m high along the distal end, as evident in the 2013 aerial images. Interestingly, the scale of shoreline displacement observed during 1952-1972 is greater than anything seen in the rest of the 45 years of aerial photograph records (Figure 7a).

Also, it is possible that transport of sediment into Dublin Bay through offshore/nearshore currents and the construction of the Dublin Port South Wall during the late 18th century and North Wall during the mid 19th century, might have triggered the trapping of sediment and net deposition of sand along its northern sector which may have resulted in the formation of a smaller island as evident in the 1819 maps (Flood, 1975; Harris, 1977) and have developed eventually into continuous sand spit. The differing shoreline accretion behaviour along coastal reaches A, B, and C is probably ascribable to the net clockwise currents (Flood, 1975; Harris, 1977; RPS, 2009) acting in the bay paired with the position of the Dublin Port North Wall and it might have been one of the major controls on the development and shape of sand dunes. However, further research is required to better understand the hydrodynamic and aerodynamic processes acting on this highly dynamic coastal land form and its evolution.

ERT surveys combined with geotechnical data have been used previously in the characterisation of coastal environments (Tronicke *et al.,* 1999; Cassiani *et al.,* 2006; Schrott and Sass, 2008). Stacking was used for data collection with four cycles and a quality factor of 5% (Peter-Borie *et al.,* 2011). Contact resistance values obtained before data collection were generally high (1000-2000 ohm). These high values were probably due to the poor conductivity given by the well sorted sands which composed the sand dunes where the electrodes were inserted. However, the aim of the resistivity imaging was to achieve qualitative information on the subsurface configuration, especially about the depth-to-bedrock and the interface between aeolian and marine/glacial sediments. In our opinion, the depicted resistivity images reasonably met that goal, although such information could only be constrained by just three nearby boreholes (see Figures 2 and 4). Thus, the depth-to-bedrock could not be ascertained for the three different sites. Accordingly, we accept that resistivity imaging did not allow us to obtain further quantitative information on the subsoil architecture, which would have required greater data coverage and rougher filtering.

The RMS error of the resistivity images was around 10%. In ideal conditions, it would have been desirable to achieve a better convergence between measured and computed pseudosections. However, it should be noted that a considerable number of noisy data were recorded during the acquisition. We attribute this to the low-resistivity of the

seawater that fills the pores and that control the bulk resistivity below sea level. In such an environment, small absolute differences in resistivity (measured during the different recording and computation cycles) might have resulted in large model residuals. For that reason, we were cautious with the data filtering to avoid eliminating geologically relevant information. Also, attempts were made to achieve a lower RMS error by a rougher data filtering. However, the geological information resulting from the ERT profile was not much different.

High environmental salinity in coastal areas may reduce meaningful interpretation of resistivity profiles. Zarroca *et al.* (2011) noted that resistivity units delineated in saline intrusion conditions may not correspond with the stratigraphic units, since the high salinity of the fluid governs the bulk resistivity. However, with the support of a detailed geomorphological map and geotechnical information, ERT has proven effective in the study of these environments (Nowroozi *et al.,* 1999; Zarroca *et al.,* 2011, 2014). As shown in Figures 4 and 5, ERT surveys were used to characterise three main hydrostratigraphic units across the study area. Aeolian and marine sediments composed of sands with thickness reaching up to 9m, overlying a lower resistivity unit interpreted as till deposits with thicknesses ranging from 10 to 20m and bedrock underlying the whole section. These data indicate that Bull Island developed over a gently undulating till plain, first as a sand bar that gradually evolved into small islands (e.g., Green Island on the north-eastern sector, see Figure 3). The construction of the Dublin Port North Wall in the mid-19th century was required to stop the progradation of marine deposits into Dublin Port. The presence of the wall, therefore, intensified sediment accumulation along its northern sector, which accelerated the process of joining the small islands into the current sand spit.

Previous studies conducted in coastal areas have shown that the GPR method could be used to provide detailed subsurface cross sections of beach ridges, aeolian dunes and shore-face sediments, providing insights on the geomorphological evolution of coastal landscapes (Jol *et al.,* 1994; Bristow *et al.,* 2000; Neal *et al.,* 2002; Choi *et al.,* 2013). GPR data presented in this work (Figure 6) show moderately continuous reflectors dipping south-eastwards indicative of dune foreslope accretion in this direction. These reflectors, particularly conspicuous in Site 1 (Figures 4 and 6), consist of continuous seaward gently dipping reflectors interpreted as beach/sand bar deposits and illustrate sand bar deposits gradually evolving into continuous foredunes. Several truncated foreslope reflectors at 70m, 220m and 390m along GPR 1 are indicative of erosive episodes probably related to significant storm events. Furthermore, sand dunes in Green Island depicted from 100m to 120m along the GPR-3 profile (Figures 4 and 6) show circular foredune development, confirming that this island was formed independently at an earlier stage than the parallel dune ridges to the east. Most probably dunes to the southeast of Green Island formed at a later stage and merged to the east of Green Island as a single ridge.

The most important controls on the long-term evolution of Bull Island are bedrock topography and accretion rate, sediment supply, and the presence of the Sutton Creek inlet along the distal end and rate of relative sea level rise. Over the long run, the balance

between sediment supply and rate of sea level rise is crucial for the evolution of Bull Island. As noted earlier, presently the accretion rate shows an increasing trend, and there are models that project that the sea-level could rise by as much as a metre over the next hundred years (Devoy, 2008; RPS, 2009). This, in combination with the south-western and western storm surge events during autumn and winter, could result in the scarping of the soft cliffs along south-eastern Irish coastlines which comprises of unconsolidated glacial deposits such as till. This might be released back to the littoral zone, and may result in the increased supply of sediment available for transport by tidal currents in a north-easterly direction. Further research into hydrodynamic and sediment transport modelling will be needed to better understand the response of nearshore beach dune systems to sea level rise.

North-eastern progradation of the distal end of Bull Island will be limited by the inlet of Sutton Creek and the volume of water discharged through the inlet from the ebb to flood tide (tidal prism). Based on shoreline change rate analysis, the north-eastern end of the spit has regressed about 100m during the period mapped using vegetation line as a shoreline proxy (Figures 3 and 7). Much of the inlet is controlled by the bedrock along the sand spit platform and the channel itself seems to be bedrock controlled. In the period mapped, there was little evidence of major changes related to inlet dynamics. Additionally, the most significant changes were the gradual build-up of a beach ridge system over the supratidal embayment.

The scenario presented above for the next 50 years (Figure 7b) is based on the continuing stability of the shorelines and sufficient sediment supply. There remains the possibility that a catastrophic storm could breach the foredune, producing extreme overwash and a situation similar to that which existed in the 18th century. However, the possibility of such a response may have been considerably reduced by the height and width of the foredune system. Presently, Bull island is part of Dublin bay biosphere reserve that has developed under a management regime that has drastically reduced destabilisation of the foredune vegetation. A major category 3 Hurricane (Ophelia), on 16th October 2017, and Storm Brian, on 20th October 2017, which lead to drastic erosion of the beach dune system along the west coast of Ireland, resulted in cliffing of the foredune and erosion of beach and foredune along Bull Island, but did not result in any breaching or overwash.

Another possible scenario could be the development of blowouts and parabolic dune formation as the foredune volume increases over time. Blowouts might occur when the vegetation cover is weakened, reduced or dies following prolonged drought (Forbes *et al.,* 2004; Davidson-Arnott, 2005; Mathew *et al.,* 2010; Ollerhead *et al.,* 2012). Once these blowouts become larger over time, they may even evolve into parabolic dunes. Currently, there are several blowouts towards the distal end of Bull Island. As shown in Figure 8, since the inland dunes are fully stabilised with the colonisation of native Marram grass species and the availability of sufficient moisture content to sustain its growth and an abundant supply of sediment through aeolian transport, the chances of these blowouts becoming larger are low.

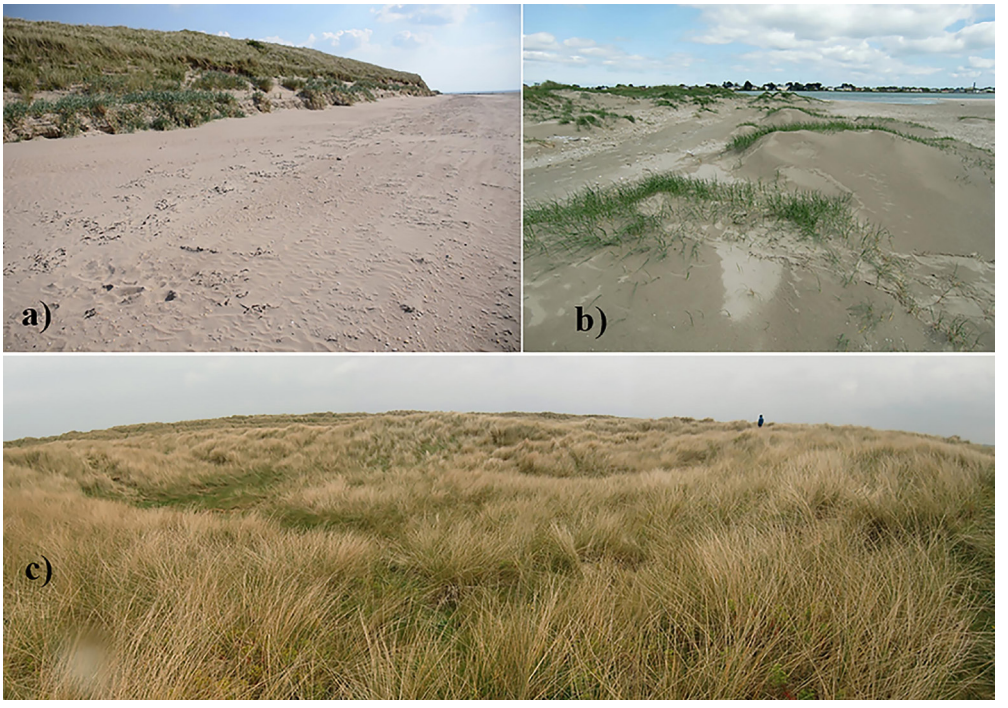

Figure 8: Photograph taken on 16/11/2017 looking north-east to the distal end of Bull Island showing: (a) continuous modern beach foredune system (6-8m) stabilised with marram grass; (b) incipient embryodunes on the beach with migrating marram grass; (c) fully stabilised inland dune complex.

Conclusions

This investigation was undertaken with the main objectives of quantifying the evolution of Bull Island. Digital photogrammetric approaches were used to determine the shoreline change rates and major geomorphological units from an analysis of historic/recent aerial/satellite images. Results from this investigation show that the availability of historic/recent aerial/satellite imagery could be used to visualise and analyse the changes in shoreline position and changes in geomorphic units of sandy beach and dune systems. In addition, geophysical approaches such as ERT and GPR supported by geotechnical data aided us to describe the subsurface physical properties of Bull Island. The ERT data was particularly useful for providing information on hydrostratigraphy and helped us to infer depth-to-bedrock. GPR allowed detailed mapping of aeolian sediment thickness and facies associations in shallower areas. Although this investigation focussed primarily on the evolution of Bull Island using geophysics and photogrammetric techniques, the approaches and methodology developed in this investigation could have numerous applications in coastal zone monitoring and management in other areas of

the world. As interest in and concern about global warming and rising sea levels on the world's coastlines continue to increase, an understanding of past behaviour of coastal systems, including rates and mechanisms driving change, is critical to future coastal zone monitoring, planning and management.

Acknowledgements

This investigation was funded by the Geological Survey Ireland INFOMAR Sea bed mapping programme. The authors are grateful to the reviewers and the editor for their constructive comments and suggestions. The reviews were detailed and helpful in improving an earlier version of this manuscript. The authors would like to thank the OSI and the OPW for providing access to the historic and recent aerial imageries, and staff in Bull Island for granting permission to carry out geophysical surveys as well as the Department of Geography of NUI Maynooth for sharing geophysical instruments used for this investigation.

References

Aagaard, T., Davidson-Arnott, R.G.D, Greenwood, B. and Nielson, J., 2004. Sediment supply from shore-face to dunes: linking sediment transport measurements and long-term morphological evolution. *Geomorphology*, 60, 205-224.

Ahn, Y., Shin, B. and Kim, K.-H., 2017. Shoreline Change Monitoring using High Resolution Digital Photogrammetric Technique. *Journal of Coastal Research*, Special Issue 79, 204-208.

Ballantyne, C.K., McCarroll, D. and Stone, J.O., 2006. Vertical dimensions and age of the Wicklow Mountains ice dome, eastern Ireland, and implications for the extent of the last Irish Ice Sheet. *Quaternary Science Reviews*, 25, 2048-2058

Bennett, M.R., Cassidy, N.J. and Pile, J., 2009. Internal structure of a barrier beach as revealed by ground penetrating radar (GPR): Chesil beach, UK. *Geomorphology* 104, 218-229.

Blue, B. and Kench, P.S., 2017. Multi-decadal shoreline change and beach connectivity in a high-energy sand system. *New Zealand Journal of Marine and Freshwater Research*, 51(3), 406-426.

Bristow, C.S. and Pucillo, K., 2006. Quantifying rates of coastal progradation from sediment volume using GPR and OSL: the Holocene fill of Guichen Bay, south-east South Australia. *Sedimentology*, 53(4), 769-788.

Bristow, C.S., Chroston, P.N. and Bailey, S.D., 2000. The structure and development of foredunes on a locally prograding coast: insights from ground-penetrating radar surveys, Norfolk, UK. *Sedimentology* 47, 923-944.

Brunn, P., 1962. Sea level rise as a cause of shore erosion. Journal of waterways, and harbours division, *ASCE*, 88, 117-130.

Buynevich, I., Bitinas, A. and Pupienis, D., 2007. Reactivation of coastal dunes documented by subsurface imaging of the Great Dune Ridge, Lithuania. *Journal of Coastal Research*, Special Edition 50: 226-230.

Carter, R.W.G. and Orford, J.D., 1988. The impact of man on the coast of Ireland. In: J. Walker, (Ed), *Artificial Structures on Shorelines*. D.H. Reidel, The Hague, 155-64.

Cassiani, G., Bruno, V., Villa, A., Fusi, N. and Binley, A.M., 2006. A saline trace test monitored via time-lapse surface electrical resistivity tomography. *Journal of Applied Geophysics*, 59, 244-259.

Choi, K.H., Choi, J.-H. and Kim, J.W., 2013. Reconstruction of Holocene coastal progradation on the east coast of Korea based on OSL dating and GPR surveys of beach-foredune ridges. *The Holocene*, 24(1), 24-34.

Constable, S., Parker, R.L. and Constable, C.G., 1987. Occam's inversion: a practical algorithm for generating smooth models from electromagnetic sounding data. *Geophysics,* 52, 289-300.

Coulouma, G., Lagacherie, P., Samyn, K. and Grandjean, G., 2013. Comparisons of dry ERT, diachronic ERT and the spectral analysis of surface waves for estimating bedrock depth in various Mediterranean landscapes. *Geoderma,* 199, 128-134.

Cunningham, A.C., Bakker, M.A.J., van Heteren, S., van der Valk, B., van der Spek, A.J.F., Schaart, D.R. and Wallinga, J., 2011. Extracting storm-surge data from coastal dunes for improved assessment of flood risk. *Geology,* 39, 1063-1066.

Davidson-Arnott, R.G.D., 2005. Conceptual model of the effects of sea-level rise on sandy coasts. *Journal of Coastal Research*, 21(6): 1166-1172.

De Franco, R., Biella, G., Tosi, L., Teatini, P., Lozej, A., Chiozzotto, B., Giada, M., Rizzetto, F., Claude, C., Mayer, A., Bassan, V. and Gasparetto-Stori, G., 2009. Monitoring the saltwater intrusion by time lapse electrical resistivity tomography: The Chioggia test site (Venice Lagoon, Italy). *Journal of Applied Geophysics*, 69, 117-130.

Devoy, R.J.N., 2008. Coastal vulnerability and the implications of sea-level rise for Ireland. *Journal of Coastal Research*, 24(2), 325-341

Eulie, D.O., Walsh, J.P., Corbett, D.R. and Mulligan, R.P., 2017. Temporal and Spatial Dynamics of Estuarine Shoreline Change in the Albemarle-Pamlico Estuarine System, North Carolina, USA. *Estuaries and Coasts*, 40(3), 741-757.

Farrell, E.R., Coxon, P., Doff, D.H. and Pried'homme, L., 1995. The genesis of the brown boulder clay of Dublin. *Quarterly Journal of Engineering Geology and Hydrogeology*, 28(2), 143-152.

Flood, D.T., 1975. The Birth of the Bull Island. *Dublin Historical Record*, Vol. 28, No. 4, 142-153.

Forbes, D.L., Parkes, G.S., Manson, G.K. and Ketch, L.A., 2004. Storms and shoreline retreat in the southern Gulf of St. Lawrence. *Marine Geology*, 210: 169-204.

Harris, C.R., 1977. Sedimentology and Geomorphology. In: D.W. Jeffrey, (Ed), *The North Bull Island, Dublin Bay, a modern coastal natural history*, The Royal Dublin Society. Dublin.

Harris, C.R., 1980. Recent Sediment Distribution in Dublin Bay and its Approaches. *Journal of Earth Sciences*, 3 (1), 41-52.

Havholm, K.G., Ames, D.V., Whittecar, G.R., Wenell, B.A., Riggs, S.R., Jol, H.M., Berger, G.W. and Holmes, M.A., 2004. Stratigraphy of Back-Barrier Coastal Dunes, Northern North Carolina and Southern Virginia. *Journal of Coastal Research*, 204, 980-999.

Houser, C. and Mathew, S., 2011. Alongshore variation in foredune height in response to transport potential and sediment supply: South Padres Island, Texas. *Geomorphology*, 125, 62-72.

Johnstone, E., Raymond, J., Olsen, M.J. and Driscoll, N., 2016. Morphological Expressions of Coastal Cliff Erosion Processes in San Diego County. *Journal of Coastal Research*, Special Issue 76, 174-184.

Jol, H.M., Meyers, R.A., Lawton, D.C. and Smith, D.G., 1994. A Detailed Ground Penetrating Radar Investigation of a Coastal Barrier Spit, Long Beach, Washington, U.S.A. In: Society of Exploration Geophysicists, (Eds), *Symposium on the Application of Geophysics to Engineering and Environmental Problems*. EEGS, 107-127.

Kandrot, S., Farrel, E.F. and Devoy, R.J.N., 2016. The morphological response of foredunes at a breached barrier system to winter 2013/2014 storms on the southwest coast of Ireland. *Earth Surface Processes and Landforms*, 41(14), 2123-2136.

LaBrecque, D., Miletto, M., Daily, W., Ramirez, A. and Owen, E., 1996. The effects of noise on Occam's inversion of resistivity tomography data. *Geophysics,* 61, 538-548.

Mathew, S., Davidson-Arnott, R.G.D. and Ollerhead, J., 2010. Evolution of beach-dune system following a catastrophic storm overwash event: Greenwich Dunes, Prince Edward Island, 1936-2005. *Canadian Journal of Earth Science,* 47, 273-290.

MET-Eireann, 2017. Windrose Dublin Airport 1-Jan-1942 to 31-Dec-2014. https://www.met.ie/climate-ireland/wind.asp# (last accessed on 21/11/2017).

Moore, L.J., 2000. Shoreline mapping techniques. *Journal of Coastal Research*, 16, 111-124.

Mulrennan, M.E., 1992. Ridge and runnel morphodynamics: an example from the central east coast of Ireland. *Journal of Coastal Research*, 8(4), 906-18.

Mulrennan, M.E., 1993. Changes since the Nineteenth Century to the Estuary-Barrier Complexes of North County Dublin. *Irish Geography*, 26(1), 1-13.

Neal, A., Pontee, N.I., Pye, K. and Richards, J., 2002. Internal structure of mixed-sand-and-gravel beach deposits revealed using ground-penetrating radar. *Sedimentology*, 49, 789-804.

Neal, A., 2004. Ground-penetrating radar and its use in sedimentology: principles, problems and progress. Earth-Science Reviews 66 (2004) 261–330.

Nowroozi, A.A., Horrocks, S.B. and Henderson, P., 1999. Saltwater intrusion into the freshwater aquifer in the eastern shore of Virginia: A reconnaissance electrical resistivity survey. *Journal of Applied Geophysics*, 42, 122.

Ollerhead, J., Davidson-Arnott, R.G.D., Walker, I.J. and Mathew, S., 2012. Annual to decadal morphodynamics of the foredune system at Greenwich Dunes, Prince Edward Island, Canada. *Earth Surface Process and Forms*, 38, 284-298.

Paine, J.G., Mathew, S. and Caudle, T., 2012. Historic shoreline change through 2007, Texas Gulf Coast: rates, contributing causes, and Holocene context. *Journal of Gulf Coast Association of Geological Societies,* 1, 13-25.

Pellicer, X.M., 2008. *Quaternary Geology of County Dublin: a description to accompany the Quaternary Geology Map of County Dublin*. Unpublished report, Geological Survey of Ireland.

Pellicer, X.M. and Gibson, P., 2011. Electrical resistivity and ground penetrating radar for the characterisation of the internal architecture of Quaternary sediments in the Midlands of Ireland. *Journal of Applied Geophysics*, 75, 638-647.

Peter-Borie, M., Sirieix, C., Naudet, V. and Riss, J., 2011. Electrical resistivity monitoring with buried electrodes and cables: noise estimation with repeatability tests. *Journal of Near Surface Geophysics*, 9(4), 369-380.

RPS, 2009. *Environmental report of the draft Dublin city development plan 2011-2017 Strategic Environmental Assessment.* Dublin City Council, Dublin.

Schrott, L. and Sass, O., 2008. Application of field geophysics in geomorphology: Advances and limitations exemplified by case studies. *Geomorphology,* 93, 55-73.

Thieler, E.R., Himmelstoss, E.A., Zichichi, J.L. and Ergul, A., 2017. Digital Shoreline Analysis System (DSAS) version 4.3 – An ArcGIS extension for calculating shoreline change: *USGS Open-File Report 2008-1278*. U.S. Geological Survey, Washington, D.C.

Tronicke, J., Blindow, N., Groß, R. and Lange, M.A., 1999. Joint application of surface electrical resistivity – and GPR-measurements for groundwater exploration on the island of Spiekeroog – northern Germany. *Journal of Hydrology*, 223, 44-53.

Zarroca, M., Bach, J., Linares, R. and Pellicer, X.M., 2011. Electrical methods (VES and ERT) for identifying, mapping and monitoring different saline domains in a coastal plain region (Alt Empordà, Northern Spain). *Journal of Hydrology*, 409, 407-422.

Zarroca, M., Linares, R., Rodellas, V., Garcia-Orellana, J., Roqué, C., Bach, J. and Masqué, P., 2014. Delineating coastal groundwater discharge processes in a wetland area by means of electrical resistivity imaging, 224Ra and 222Rn. *Hydrological Processes*, 28(4), 2382-2395.